frontiers | Frontiers in Physics

A multi-wavelength mid-IR laser based on $BaGa_4Se_7$ optical parametric oscillators

Minqiang Kang[1], Zhenguo Wang[1], Jianbin Li[1], Xinying Jiang[1],
Kaibo Xiao[1], Song Zhou[1], Fan Zhang[1], Xiangjun Xiang[1],
Zhitao Peng[1], Jiyong Yao[2]*, Qihua Zhu[1]* and Guoying Feng[3]*

[1]Research Center of Laser Fusion, China Academy of Engineering Physics, Mianyang, China, [2]Center for Crystal Research and Development, Key Laboratory of Functional Crystals and Laser Technology, Technical Institute of Physics and Chemistry, Chinese Academy of Sciences, Beijing, China , [3]Institute of Laser and Micro/Nano Engineering, College of Electronics and Information Engineering, Sichuan University, Chengdu, Sichuan, China

A multi-wavelength mid-IR laser consisting of 3.05 μm, 4.25 μm, and 5.47 μm $BaGa_4Se_7$(BGSe)optical parametric oscillators (OPOs) switched by DKDP electro-optic switches with one 10 Hz/7.6 ns pumping wave is demonstrated. Maximum energies at 3.05 μm, 4.25 μm, and 5.47 μm are 1.35 mJ, 1.03 mJ, and 0.56 mJ, respectively, corresponding to optical-to-optical conversion efficiencies of 9.4%, 7.6%, and 4.2%. To the best of our knowledge, this study is the first of generation of three mid-IR wavelength lasers using electro-optic switches. Furthermore, this study provides a viable solution for a high-energy or high-power, compact, or even portable multi-wavelength mid-IR laser device that employs a single pumping wave.

1 Introduction

The mid-IR lasers are highly transparent in the atmosphere and possess absorption peaks that overlap with many atoms and molecules, making them suitable for various applications such as spectroscopy, remote sensing, medical treatment, communication, industry, scientific research, etc. [1–10]. In certain situations, a mid-IR laser with a multi wavelengths will be needed, such as for remote sensing detection of different harmful gases, layered processing of multilayer organic matter, and so forth [11, 12]. A multi-wavelength mid-infrared laser source is necessary in these situations. There are not many reports on this laser source, though. The primary focus of this study is on this kind of laser source.

There are many approaches to achieving mid-IR lasers, such as chemistry lasers, free electron lasers, quantum cascade lasers, gas lasers, solid state lasers, fiber lasers, non-linear optical frequency conversion of optical parametric oscillator (OPO) and optical parametric amplifier (OPA), and so on [13–17]. Among them, OPO is a relatively easy method to obtain high energy, high power, and high beam quality, along with a relatively compact and wide tuning range [18–24]. However, its wavelength coverage has been limited by the availability of suitable non-linear optical crystals. Furthermore, for mid-IR outputs, long-wavelength pumping waves are usually required to fulfil phase matching conditions. Currently, many non-linear optical (NLO) crystals (oxide and non-oxide) have been investigated for the mid-
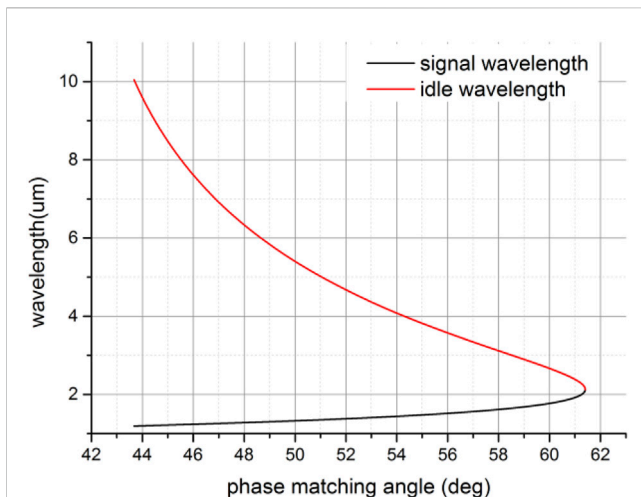
FIGURE 1
Type-I phase matching curve of OPO by 1064 nm pumping in BGSe.

IR region [7]. BGSe crystal is one of the most promising NLO crystal for mid-IR laser generation. It has a wide band gap (2.64 eV) and a wide transparency spectrum (0.47–18 μm) [8–10]. The BGSe has been extensively used in OPO operation in the mid-IR region, pumped by economical ~1 μm laser sources [14–19]. Feng Yang et al. presented three high pulse energy BGSe OPOs pumped by a 1064 nm laser; the maximum pulse energy at 3.9 μm is 0.83 mJ with a 9.1 mJ pumping wave, the maximum pulse energy at 3.0 μm is 1.0 mJ, and the maximum pulse energy at 5.0 μm is 0.3 mJ with an 8.2 mJ pumping wave; the optical efficiency are 12.2% at 3.0 μm, 9.1% at 3.9 μm, 3.75% at 5.0 μm, and in their experiment which the three mid-IR laser OPOs are independent [22], they need to manually to change the pumping wave to get the three mid-IR waves, which is not benefit to compact or even portable mid-IR laser source. Wen-Tao Xu et al. used the same BGSe OPO pumped by a 1064 nm laser source and achieved the maximum pulse energy at 4.11 μm of 2.56 mJ with the pumping pulse energy of 61.6 mJ; correspondingly, the optical efficiency is 4.2% at 4.11 μm, and the mid-IR laser is tuned between 3.12 μm and 5.16 μm. And in Wen-Tao Xu's experiment, as the mid-IR waves are tuned with the same NLO crystal and the same optical lens, in particular the crystal cutting angle is fixed, which is not conducive to the improvement of conversion efficiency for all the signal and idle waves in the long tuning ranges [23].

In our study, a multi-wavelength mid-IR laser of 3.05 μm, 4.25 μm, and 5.47 BGSe OPOs switched by DKDP electro optic switches with one 10 Hz/7.6 ns pumping is demonstrated. The maximum energies at 3.05 μm, 4.25 μm, and 5.47 μm are 1.35 mJ, 1.03 mJ, and 0.56 mJ, corresponding to optical-to-optical conversion efficiencies of 9.4%, 7.6%, and 4.2%, respectively. By the method of our study, it provides a viable solution for a high-energy or high-power, compact, or even portable multi-wavelength mid-IR laser source that employs a single pumping wave. And any waves in the range of the OPO's can be achieved by appropriate crystal cutting.

2 Phase matching and experimental setup

The BGSe crystal belongs to the monoclinic system (m-point group), and it is a biaxial crystal. The Type-I phase matching conditions (o → e + e) for the BGSe crystal are calculated in the x-z plane, the phase matching curve of OPO by 1064 nm pumping in BGSe is shown in Figure 1. As it is shown, when the matching angle is cut at 49°, 53°, or 59°, the BGSe OPO can output an idle wave of 5.5 μm, 4.2 μm, or 3.0 μm. And in our experiment, the three angles are 48.5°, 53.2°, and 59.4°, respectively.

The pumping wave is a 808 nm diode side pumped Q-switched Nd:YAG pulse laser with a repetition frequency of 10 Hz. It is a plane-plane cavity; M1 is a highly reflective (HR) mirror coated at 1064 nm; a polarizer (P1) and a quarter-wave plate (QWP) are used to choose the line-polarized light for passing through the Pockels cell PC1; and M2 is a partially reflective (PR) mirror coated at 1064 nm with a transparency efficiency of 50%. The cavity length of the pumping wave is as short as possible, at 200 mm.

The experimental configuration is shown in Figure 2. It is composed of the pumping wave, the three OPO cavities, and the trigger pulse generator.

The pumping wave is initially reflected by a 45° plane HR mirror, which is coated at 1064 nm (R > 99.5%), and subsequently transmitted through a half-wave plate (HWP) and then passed through a Pockels cell PC2. By using the PC2 and the polarizer P2, the pumping pulse is switched among the OPO cavity-1, cavity-2, and cavity-3. The pumping pulse is switched between the OPO cavities two and three using the Pockels cell PC3 and the polarizer P3. The three half-wave plates before the three OPO cavities are employed to get the appropriate polarized direction to make the three BGSe OPOs set at o-ee type-I phase matching.

The BGSe OPO cavity consisted of a pair of flat mirrors and a BGSe crystal. For the 3 μm mid-IR laser in the OPO cavity-1, the input mirror M5 is antireflection (AR) coated at 1064 nm on the input surface, high-reflection (HR) coated at 2.4 μm–3.3 μm, and high-transmission (HT) coated at 1064 nm on the output surface. To increase the utilisation of the pump energy (and thus improve conversion efficiency), the output coupler M6 is high-reflection coated at 1064 nm (R > 99%), achieving about 20% transmission in the range of 2.4 μm–3.3 μm for idle waves to obtain a high output energy. The BGSe1 with dimensions of 8 mm³ × 8 mm³ × 10 mm³ and AR-coatings on both surfaces, is cut in the x-z plane at $\theta = 59.4°$ and $\varphi = 0°$ for o-ee type-I phase matching, set parallel to the y-axis with an 8 mm edge. For the 4 μm mid-IR laser in the OPO cavity-2, the M7 is also AR coated at 1064 nm on the input surface, HR coated at 3.8 μm–4.7 μm, and HT coated at 1064 nm on the output surface. The output coupler M8 is HR coated at 1064 nm (R > 99%), and 20% transmission coated in the range of 3.8 μm–4.7 μm. The BGSe2, also with dimensions of 8 mm³ × 8 mm³ × 10 mm³ and AR-coatings on both surfaces, is cut in the x-z plane at $\theta = 53.2°$ and $\varphi = 0°$ for o-ee type-I phase matching and set parallel to the y-axis with an 8 mm edge. And for the 5 μm mid-IR laser in the OPO cavity-3, the M9 is also AR coated at 1064 nm on the input surface, HR coated at 5.0 μm–6.5 μm, and AR coated at 1064 nm on the output surface. The output coupler M10 is HR coated at 1064 nm (R > 99%) and 20% transmission coated in the range of 5.0 μm–6.5 μm. The BGSe3, also with dimensions of 8 mm³ × 8 mm³ × 10 mm³ and AR-coatings
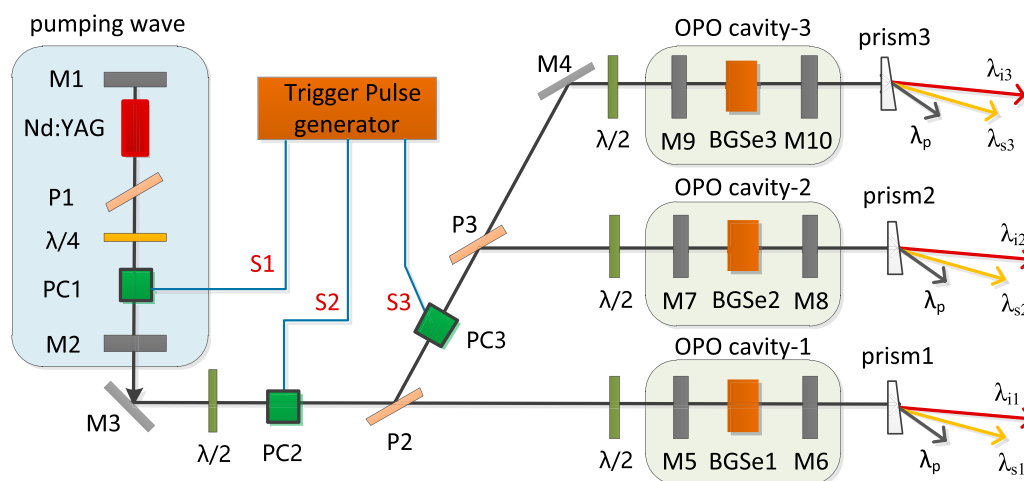
FIGURE 2
The experimental configuration of the multi-wavelength mid-IR BGSe OPO, λ_p is pumping wave, λ_{sm} (m = 1, 2, 3) is signal wave, λ_{im} (m = 1, 2, 3) is idle wave.
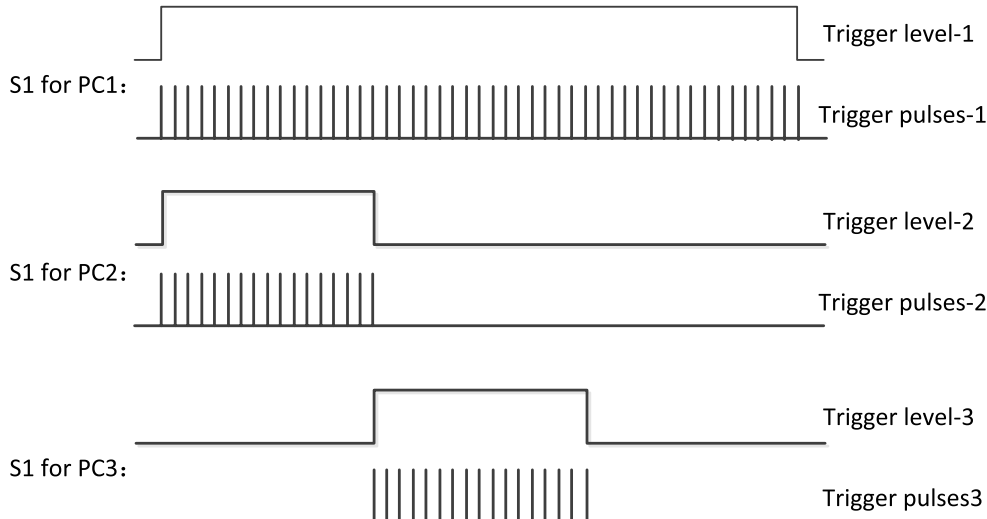

FIGURE 3
The trigger pulse sequences for PC1, PC2, and PC3.

on both surfaces, is cut in the x-z plane at $\theta = 48.5°$ and $\varphi = 0°$ for o-ee type-I phase matching, set parallel to the y-axis with an 8 mm edge. For separating the idle and signal waves, three CaF_2 prisms with a 30° angle without coating are used near the three output-coupling mirrors of M6, M8, and M10.

The pumping wave is switched among the three BGSe OPOs by the trigger pulses of S1, S2, and S3 generated by a trigger pulse generator operated at a pulse repetition frequency of 10 Hz. The trigger pulse generator which is composed by a synchronizer and a digital signal generator. The trigger pulse sequences for PC1, PC2, and PC3 are shown in Figure 3. The trigger level-1 for S1 is all the way up, the gate width of the trigger level-2 for S2 is 250 ns, and the

level is high-low-low; the gate of the trigger level-3 for S3 is the same 250 ns, and the level is low-high-low. The PC1, PC2, and PC3 are all DKDP crystals, the clear aperture is 10 mm × 10 mm, and the driving half-wave voltage is 3.4 kV, which is flat topping square with the rise time $\not> 10$ ns.

3 Result and discussion

The measured temporal pulse shape and spatial distribution of the pumping wave are shown in Figure 4. The beam diameter and the pulse duration of the pumping wave are 2.6 mm and 7.6 ns, respectively.
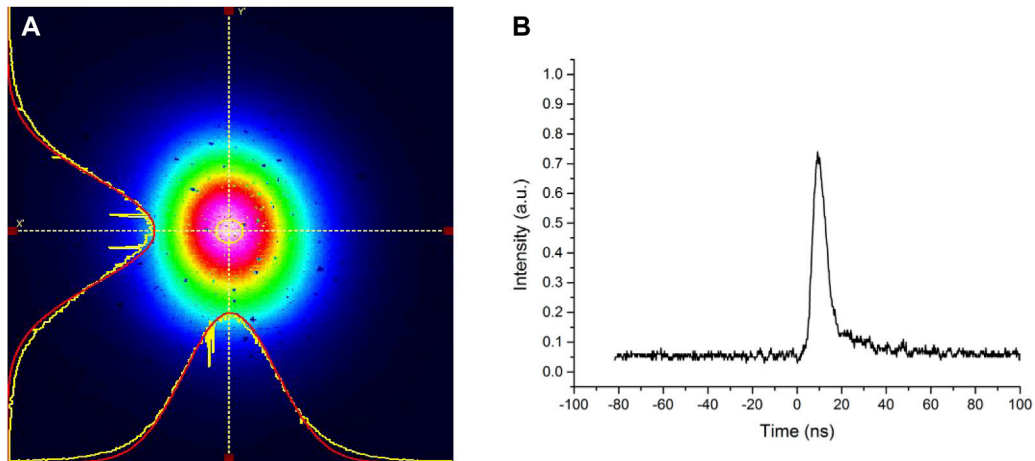
FIGURE 4
The measured temporal pulse shape and spatial distribution of the pumping wave. **(A)** The spatial distribution of the pumping wave, **(B)** The temporal pulse shape of the pumping wave.
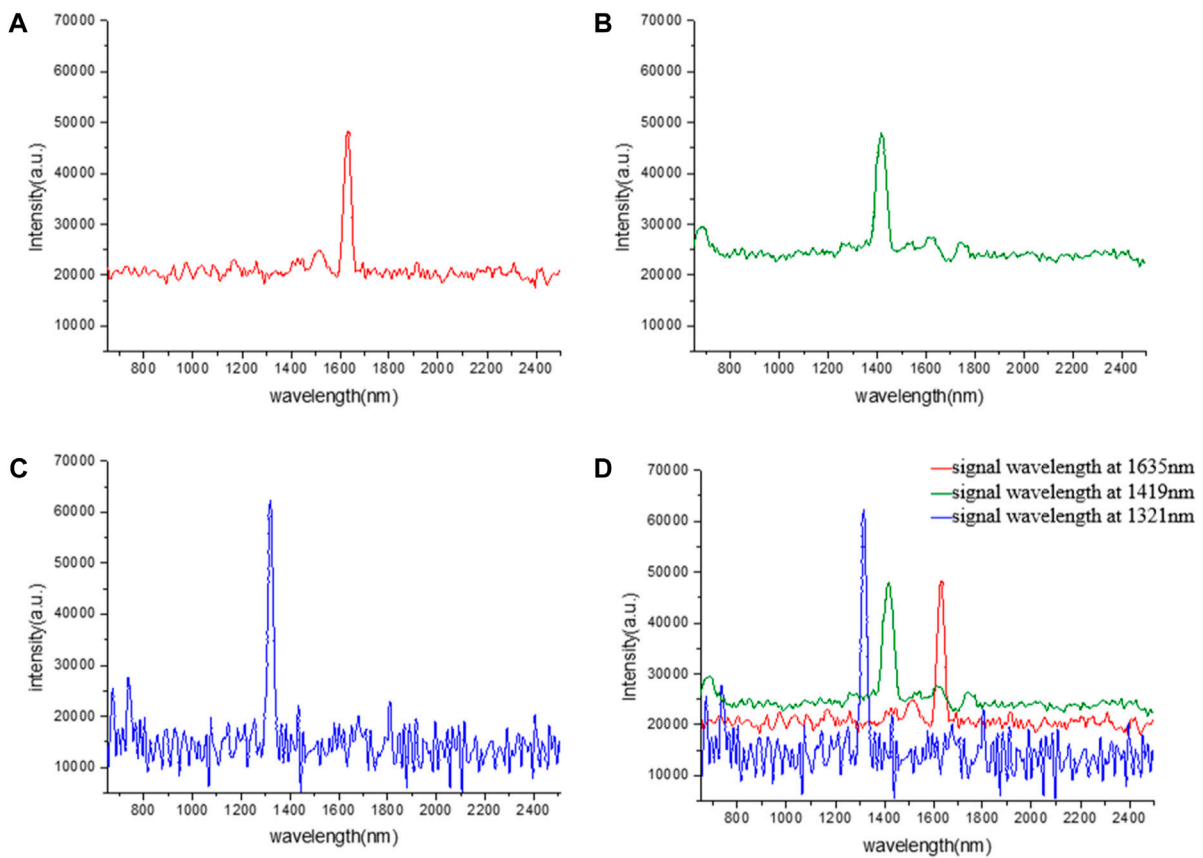
FIGURE 5
The spectrum for the three signal waves. **(A)** The spectrum for the signal wave of 1635 nm, **(B)** The spectrum for the signal wave of 1419 nm, **(C)** The spectrum for the signal wave of 1321 nm, **(D)** The spectrums for the three signal waves.

As it is shown in Figure 3, when the pumping wave is injected into the OPO cavity-1, the signal wave 1635 nm, and the idle wave 3.05 μm can be achieved; when the pumping wave is injected into the OPO cavity-2, the signal wave 1419 nm, and the idle wave 4.25 μm can be achieved; when the pumping wave is injected into the OPO cavity-3, the signal wave 1321 nm, and the idle wave 5.47 μm can be

FIGURE 6
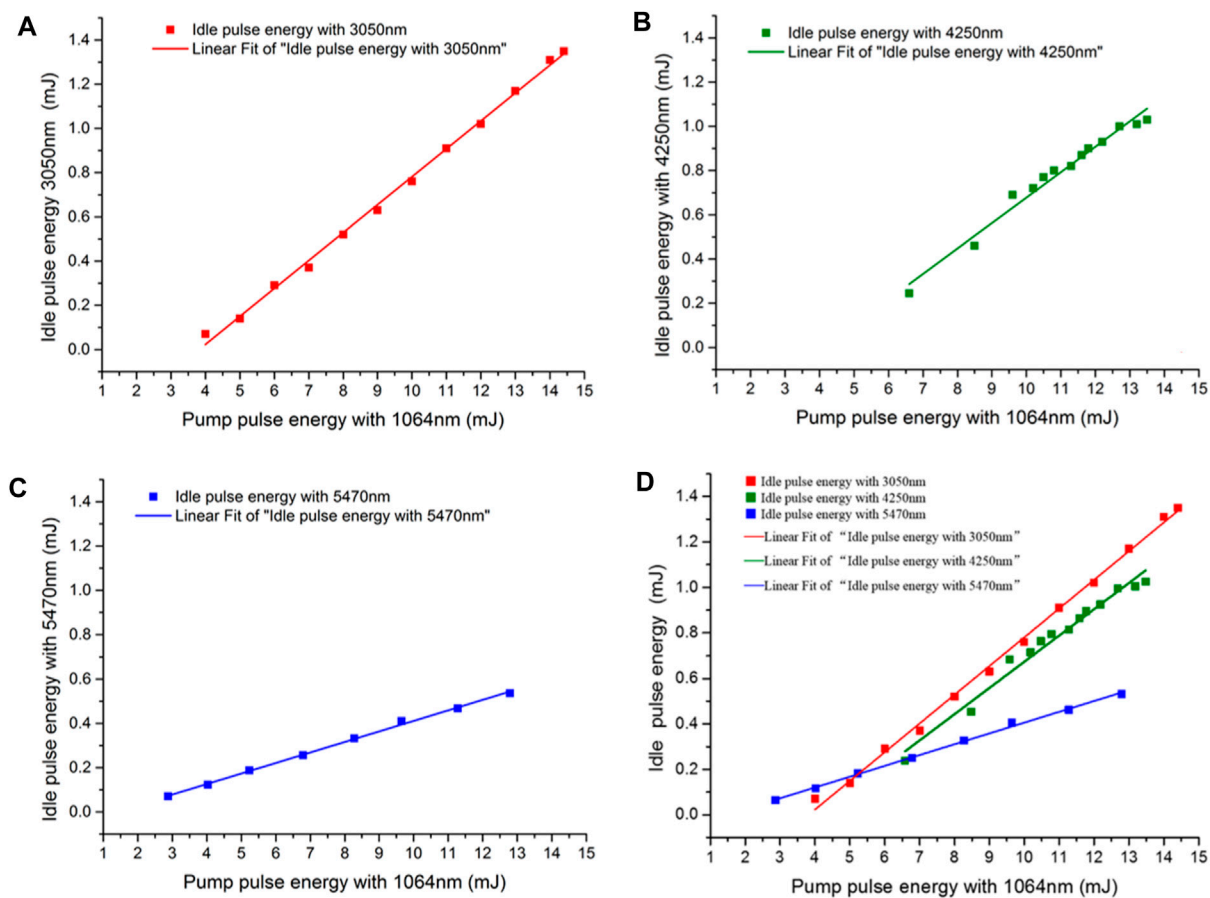The output pulse energies for three idle waves. **(A)** The output pulse energy of idle wave 3.05 μm *versus* the pulse energy of pump wave 1064 nm, **(B)** The output pulse energy of idle wave 4.25 μm *versus* the pulse energy of pump wave 1064 nm, **(C)** The output pulse energy of idle wave 5.47 μm *versus* the pulse energy of pump wave 1064 nm, **(D)** The output pulse energy of the three idle waves *versus* the pulse energy of pump wave 1064 nm.

achieved. Due to the lack of conditions for direct measurement of the idle wave spectrum in our laboratory, estimation is done by measuring the spectrum of the signal wave. And the spectrum of the signal waves is monitored by an optical spectrum analyser. The three signal waves are measured behind prisms 1, 2, and 3. As shown in Figures 5A,B,C, the spectra of the three signal waves are 1635 nm, 1419 nm, and 1321 nm, respectively. According to the OPO momentum conservation condition ($1/\lambda_p = 1/\lambda_s + 1/\lambda_i$), with the measured pump wavelength λ_p being 1064 nm and the signal wavelengths λ_s being 1635 nm, 1419 nm, and 1321 nm, in this case the idle wavelengths λ_i are calculated to be 3.05 μm, 4.25 μm, and 5.47 μm, respectively. The spectrums for the three signal waves are shown in Figure 5D.

The energy of the idle waves is monitored by an energy calorimeter. The energies of the three idle waves output *versus* the 1064 nm pump energy are shown in Figures 6A,B,C. As depicted in Figure 6, the output idle energy increases with the injected pump energy. As it is shown in Figure 6A, the threshold pulse energy of the 3.05 μm wave is about 4 mJ, which corresponds to the energy fluence of 0.075 J/cm² and the peak intensity of 9.89 MW/cm². As it is shown in Figure 6B, the threshold pulse

energy of the 4.25 μm wave is about 5 mJ, which corresponds to the energy fluence of 0.094 J/cm² and the peak intensity of 14 MW/cm². And as it is shown in Figure 6C, the threshold pulse energy of the 5.47 μm wave is about 2.88 mJ, which corresponds to the energy fluence of 0.054 J/cm² and the peak intensity of 7.1 MW/cm². The maximum output energy of 1.35 mJ at 3.05 μm is obtained under the pump energy of 14.4 mJ, corresponding to an optical-optical conversion efficiency of 9.4% from 1.064 μm to 3.05 μm, and the slope conversion efficiency η1 is about 13.1%, which is calculated from the linear fitting curves. The maximum output energy of 1.03 mJ at 4.25 μm is obtained under the pump energy of 13.5 mJ, corresponding to an optical-optical conversion efficiency of 7.6% from 1.064 μm to 4.25 μm, and the slope conversion efficiency η2 is about 13.5%, which is calculated from the linear fitting curves. And the maximum output energy of 0.54 mJ at 5.47 μm is obtained under the pump energy of 12.8 mJ, corresponding to an optical-optical conversion efficiency is 4.2% from 1.064 μm to 5.47 μm, and the slope conversion efficiency η3 is about 6.9%, as calculated from the linear fitting curves. As shown in Figure 6D, the slope conversion efficiencies of the three idle waves are η1≈η2>η3. This is primarily due to the not good condition of our
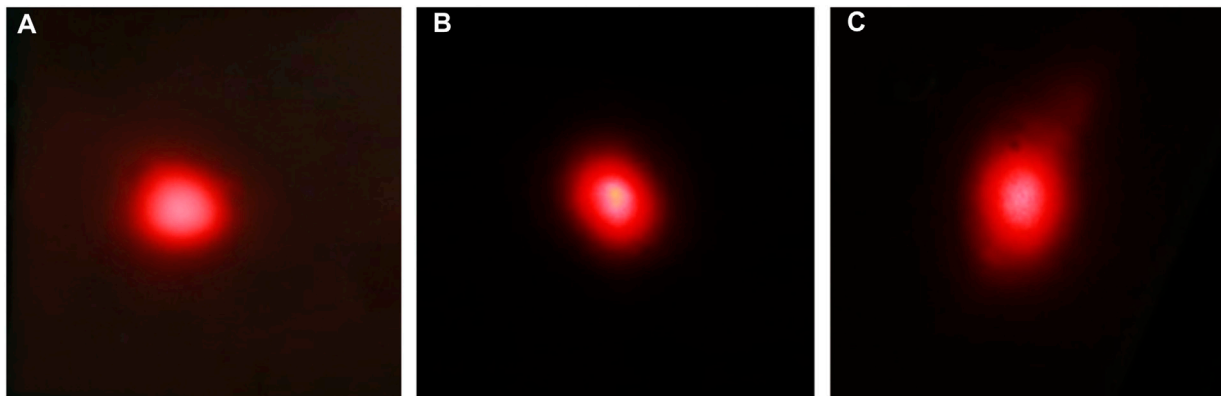
FIGURE 7
The measured spatial distribution of the signal wave by an infrared photosensitive card. **(A)** The spatial distribution of the signal wave 1288 nm, **(B)** The spatial distribution of the signal wave 1433 nm, **(C)** The spatial distribution of the signal wave 1655 nm.

BGSe1 crystal, for the coating of which has some performance degradation.

As lack of appropriate response wavelength CCD in mid-IR range in our experiment, so we do not measure the spatial distributions of the three pairs of the signal and idle waves directly. But, in order to roughly get the spatial distributions, we record the spatial distributions of the three signal waves by an infrared photosensitive card which can sensitive to the longest wavelength of 1.7 μm. And the record spatial distributions of the three signal waves are shown in Figure 7.

4 Conclusion

In our study, we demonstrated a multi-wavelength mid-IR laser of 3.05 μm, 4.25 μm, and 5.47 BGSe optical parametric oscillators (OPO) switched by DKDP electro optics switches with one 10 Hz/7.6 ns pumping wave. The maximum output pulse energies of 3.05 μm, 4.25 μm, and 5.47 μm are 1.35 mJ, 1.03 mJ, and 0.56 mJ pumped at 1.064 μm with the pulse energies of 14.4 mJ, 13.5 mJ, and 12.8 mJ, respectively. The corresponding optical-to-optical conversion efficiencies are 9.4%, 7.6%, and 4.2% and the slope conversion efficiencies of the three idle waves are 13.1%, 13.5%, and 6.9%, respectively. To the best of our knowledge, this study is the first to adopt electro-optic switches to generate three mid-IR wavelength lasers. As far as we are aware, this is the first study for the BGSe crystal that has produced three mid-IR wavelength lasers from a single pumping source utilizing electro-optic switches, which offers a good solution for high energy and compact multi-wavelength mid-IR laser generation.

Data availability statement

The original contributions presented in the study are included in the article/supplementary material, further inquiries can be directed to the corresponding authors.

Author contributions

MK: simulation calculation, experiment completion; ZW: experiment completion; JL, KX, SZ, FZ, and XX : assisted completion of the experiment; XJ: experiment completion; ZP: idea construction and check the data; JY, QZ, and GF: idea construction, check the data and revise the manuscript.

Conflict of interest

The authors declare that the research was conducted in the absence of any commercial or financial relationships that could be construed as a potential conflict of interest.

Publisher's note

All claims expressed in this article are solely those of the authors and do not necessarily represent those of their affiliated organizations, or those of the publisher, the editors and the reviewers. Any product that may be evaluated in this article, or claim that may be made by its manufacturer, is not guaranteed or endorsed by the publisher.

References

1. Chunlai L, Gang L, Liyin Y, Wang Y, Jin J, Xu Y, et al. Laboratory calibration and application of the airborne thermal infrared hyperspectral imager (ATHIS). *Infrared Laser Eng* (2020) 49(5):20190117. doi:10.3788/irla.20_2019-0117

2. Qian W, Hong-xing W, Min L. Performance and analysis of IR lasers communications through fog medium. *Sci Technol Eng* (2010) 33(10):114–5.

3. Zhang Z, Xie X, Duan T, Yu W, Wei W. Numerical calculation of 3.8 μm and 1.55 μm laser radiation transmission characteristic under foggy condition. *Infrared Laser Eng* (2016) 45(S1):S104007. doi:10.3788/irla201645s1.104007

4. Lippert E, Nicolas S, Arisholm G, Stenersen K, Rustad G. Midinfrared laser source with high power and beam quality. *Appl Opt* (2006) 45(16):3839–3845. doi:10.1364/ao.45.003839

5. Schliesser A, Picqué N, Hänsch TW. Mid-infrared frequency combs. *Nat Photon* (2012) 6:440–9. doi:10.1038/nphoton.2012.142

6. Doroshenko ME, Jelınkova H, Koranda P, Šulc J, Basiev T, Osiko V, et al. Tunable mid-infrared laser properties of Cr^{2+}:ZnMgSe and Fe^{2+}:ZnSe crystals. *Laser Phys Lett* (2010) 38(7):38–45. doi:10.1002/lapl.200910111

7. Basiev TT, Orlovskii YV, Galagan BI. Evaluation of rare-earth doped crystals and glasses for 4~5 μm lasing. *Laser Phys* (2002) 12(5):25–28.

8. Velikanov SD, Zaretskiy NA, Zotov EA, Kozlovsky VI, Korostelin YV, Krokhin ON, et al. Investigation of Fe:ZnSe laser in pulsed and repetitively pulsed regimes. *Quan Electron* (2015) 45(2):1–7. doi:10.1070/qe2015v045n01abeh015644

9. Dong XL, Zhang BT, He JL, Huang HT, Yang KJ, Xu JL, et al. High-power 1.5 and 3.4 μm intracavity KTA OPO driven by a diode-pumped Q-switched Nd:YAG laser. *Opt Commun* (2009) 1670:2821668–70. doi:10.1016/j.optcom.2008.12.071

10. Petrov V, Schunemann PG, Zawilski KT, Pollak TM. Noncritical singly resonant optical parametric oscillator operation near 62 μm based on a $CdSiP_2$ crystal pumped at 1064 nm. *Opt Lett* (2009) 34(4):2399–2401. doi:10.1364/ol.34.002399

11. Ma X, Zhiyuan Z, Hong Z. Drug spectrum analysis based on far-infrared spectroscopy. *Opt Instr* (2020) 42(2):20–25.

12. Fang S. Research of mid-infrared laser methane sensing technique. [PHD]. Changchun: Jilin University (2020).

13. Tyazhev A, Vedenyapin V, Marchev G, Isaenko L, Kolker D, Lobanov S, et al. Singly-resonant optical parametric oscillation based on the wide band-gap mid-IR nonlinear optical crystal $LiGaS_2$. *Opt Mater* (2013) 35:1612–5. doi:10.1016/j.optmat.2013.03.016

14. Yuan JH, Li C, Yao BQ. High power, tunable mid-infrared $Baga_4Se_7$ optical parametric oscillator pumped by a 2.1μm Ho:YAG laser. *Opt Express* (2016) 24(6):35–42.

15. Yao JY, Mei DJ, Bai L, Lin Z, Yin W, Fu P, et al. $Baga_4Se_7$: A new congruent-melting ir nonlinear optical. *Material"* Inorg Chem (2010) 49:9212–6. doi:10.1021/ic1006742

16. Yao JY, Yin WL, Feng K, Li X, Mei D, Lu Q, et al. Growth and characterization of $Baga_4Se_7$ crystal. *J Cryst Growth* (2012) 346(1):1–4. doi:10.1016/j.jcrysgro.2012.02.035

17. Yang F, Yao JY, Xu HY. Midinfrared optical parametric amplifier with 6.4-11 μm range based on $Baga_4Se_7$ crystal. *IEEE Photon Technol. Lett.* (2015) 27(10):1100–1103.

18. Badikov V, Badikov D, Shevyrdyaeva G, Tyazhev A, Marchev G, Panyutin V, et al. Phase-matching properties of $Baga_4S_7$ and $Baga_4Se_7$: Wide-bandgap nonlinear crystals for the mid-infrared. *Phys Status Solidi RRL* (2011) 5:31–3. doi:10.1002/pssr.201004425

19. Boursier E, Segonds P, Debray J, Inacio PL, Panyutin V, Badikov V, et al. Angle noncritical phase-matched second-harmonic generation in the monoclinic crystal $Baga_4Se_7$. *Opt Lett* (2015) 40(20):4591–4594. doi:10.1364/ol.40.004591

20. Zhang X, Yao JY, Yin WL, Zhu Y, Wu Y, Chen C. Determination of the nonlinear optical coefficients of the $Baga\_4Se\_7$ crystal. *Opt Express* (2015) 23(1):552–558. doi:10.1364/oe.23.000552

21. Kostyukova NY, Boyko AA, Badikov V, Badikov D, Shevyrdyaeva G, Panyutin V, et al. Widely tunable in the mid-IR $Baga_4Se_7$ optical parametric oscillator pumped at 1064 nm. *Opt Lett* (2016) 41(15):3667–3670. doi:10.1364/ol.41.003667

22. Yang F, Yao JY, Xu HY, Feng K, Yin W, Chen C, et al. High efficiency and high peak power picosecond mid-infrared optical parametric amplifier based on $Baga_4Se_7$ crystal. *Opt Lett* (2013) 38(19):3903–3905. doi:10.1364/ol.38.003903

23. Xu WT, Wang Y, Xu DG, Li C, Yao JY, Yan C, et al. High-pulse-energy mid-infrared optical parametric oscillator based on Baga4Se7 crystal pumped at 1.064 μm. *Appl Phys B* (2017) 123:80. doi:10.1007/s00340-016-6631-5

24. Debuisschert T, Raffy J, Pocholle J-P, Papuchon M. Intracavity optical parametric oscillator: Study of the dynamics in pulsed regime. *J Opt Soc Am B* (1996) 13:1569–1587. doi:10.1364/josab.13.001569